Journal of Superconductivity and Novel Magnetism (2019) 32:1027–1033
https://doi.org/10.1007/s10948-018-4776-7

ORIGINAL PAPER

Study of the Effect of Pr Doping on Structural, Morphological and Magnetic Properties of Nickel Ferrite

Mukesh Kumari[1] · **Mukesh Chander Bhatnagar**[1]

Received: 19 May 2018 / Accepted: 13 June 2018 / Published online: 5 July 2018

Abstract

Praseodymium rare earth ion (Pr^{3+}) doped nickel ferrite ($NiFe_{2-x}Pr_xO_4$, $0 < x < 0.1$) nanocrystals (NFPO) were synthesized by hydrothermal method. The structural, morphological and magnetic properties of the prepared samples have been studied. The x-ray diffraction (XRD) and fourier transform infrared (FTIR) techniques confirmed the phase formation of the NFPO nanocrystals. The average crystallite size of NFPO nanoparticles found to be in the range 39 to 44 nm. The presence of Pr ions in NFPO was confirmed by energy-dispersive x-ray (EDX) analysis. It has been observed that after a certain amount of Pr doping, the morphology of the nanocrystals starts changing from nano-octahedrons to nanorods shape, as confirmed by transmission electron microscopy (TEM). Also, the magnetic properties of the prepared nanocrystals were measured using physical properties measurement system (PPMS) at 10 K and 300 K. The saturation magnetization (Ms) first decreases with the increasing loading amount of Pr ions up to ($x = 0.025$) and later it increases at both the temperatures. However, the value of coercivity shows an increasing trend with the increasing amount of Pr ions in NFPO at room temperature.

Keywords Ferrites · Hydrothermal · Rare earth-doped nanoparticles · Nano-octahedrons

1 Introduction

Recently, the spinel ferrites with general formula AB_2O_4, belonging to the cubic spinel structure, have drawn huge attention due to their remarkable properties to meet the necessities of various applications. Nickel ferrite, a centrosymmetric ferrite which is a soft magnetic material with an inverse spinel structure, have a broad range of applications in many fields such as gas sensors [1], photocatalytic [2] and microwave absorber [3].

The inverse spinel structure of nickel ferrite (NFO) has 16 octahedral (B site) and 8 tetrahedral (A site) filled sites out of total 32 B sites and 64 A sites created by oxygen ions. In a unit cell of the spinel structure, there are 16 Fe^{3+}, 8 Ni^{2+} and 32 O^{2-} ions. In case of inverse spinel structure, 16 Fe^{3+} ions are equally conveyed between A and B sites. The remaining eight B sites are occupied by Ni^{2+} ions. Physical properties of the ferrites depend on cation distribution among these sites, which is very much sensitive to the method of preparation [4], particle size [5] and doping [6]. The specific nature of the dopant (semiconductor, metal) into spinel structure can also influence the final magnetic and electrical characteristics [7, 8]. The amount of this modification is decided by the ionic radius, the valency of the substituting ion and its site of preference [9–11].

Many scientific groups are working on the doping of these rare earth (RE) ions in the spinel structure because of their strong spin-orbit coupling of the angular momentum and unpaired 4f electrons. Addition of RE metal ions into the spinel structure creates strain due to distortion that can affect the structure and/or morphology [12]. In this way, the electrical and magnetic behaviour of these nano ferrites can be modified according to the application [13]. Zhiqing et al. studied the effect of Sm ions substitution on dielectric and magnetic properties of Ni–Zn ferrite [14]. Pratibha Rao et al. studied the effect of Pd incorporation on the gas sensing behaviour of NFO and reported the reduction in operating temperature and also observed faster response and recovery characteristic [15]. Xiaofei Wu et al. found the change

✉ Mukesh Kumari
mukeshdhillon20@gmail.com

[1] Indian Institute of Technology Delhi, New Delhi, 110016, India

in morphology of Cobalt ferrite by adding Pr ions [13]. Rezlescu et al. revealed that rare earth ions prefer to enter in octahedral sites by replacing Fe^{3+} ions in the lattice when doping is low and due to their larger ionic radius greatly influence the physical properties of substituted ferrite [16].

There are many methods used for the preparation of nanocrystal ferrites having their own advantages and disadvantages like sol-gel auto combustion [14], co-precipitation [6], solid-state reaction [12], mechanical ball milling [17], electrospinning [18] and hydrothermal [19]. In this work, we prepared our samples using the hydrothermal method. The hydrothermal method is broadly used due to low economic cost, low operating temperature, easy handling, a high degree of uniformity and high command on the morphology of nanomaterials [20]. Also, in the hydrothermal technique, no further sintering is required to form a phase of samples.

Here, in this work, we synthesized $NiFe_{2-x}Pr_xO_4$ ($x = 0$, 0.025, 0.05, 0.075 and 0.1) by hydrothermal method and focused on the effect of Pr substitution on structural, morphological and magnetic properties of nickel ferrite. To the best of our knowledge, there are no reports available in the literature regarding the use of Pr^{3+} ion-doped nickel spinel ferrite nanoparticles using the hydrothermal method.

2 Experimental

2.1 Chemicals

Ferric nitrate nonahydrate $Fe(No_3)_2.9H_2O$, nickel nitrate hexahydrate $Ni(No_3)_3.6H_2O$, praseodymium nitrate hexahydrate $Pr(No_3)_3.6H_20$ and sodium hydroxide (NaOH) are used as starting materials without advance purification.

2.2 Synthesis of $NiFe_{2-x}Pr_xO_4$ Nanocrystals

Nanocrystalline NFPO has been synthesized by the surfactant-free hydrothermal method. In this method, nickel nitrate hexahydrate and ferric nitrate nonahydrate + praseodymium nitrate hexahydrate has been taken in 1:2 molar ratio in deionized (DI) water and stirred for 30 min. A 3 M NaOH solution has been prepared in 20-ml DI water and added dropwise into the above solution. The solution was constantly stirred for 1 h to form a slurry. After that, the slurry was transferred to the Teflon-lined stainless steel autoclave and heated at 200 °C for 12 hrs. The final product was washed with DI water and ethanol for three to four times and then dried at 80 °C for 4 hrs. The samples of the series $NiFe_{2-x}Pr_xO_4$ ($x = 0$, 0.025, 0.050, 0.075 and 0.1) were prepared with increasing loading amount of Pr ions denoted as P0–P4, respectively.

2.3 Characterization

Nanocrystals of NFPO were characterized structurally using x-ray diffractometer (PANalytical X'pert Pro model) having CuKα radiation ($\lambda = 1.54060$ Å) in the 2θ range from 20° to 70° using Bragg-Brentano geometry ($v = 45$ kV, $I = 40$ mA). Transmission electron microscopy (FEI TecnaiTF20 and JEOL JEM-1400) were used to characterize the morphology and particle size. Magnetic measurements were carried out using a physical property measurement system (Quantum Design PPMS) with a maximum applied field range of 1 T. The chemical compositions are examined by energy-dispersive x-ray spectrophotometer (SWIFT ED-3000). Fourier transform infrared spectrometer (FTIR, Thermo Scientific Nicolet-6700) was used to record FTIR spectrum near the infrared region over the range 400 to 4000 cm^{-1}.

3 Result and Discussion

3.1 X-ray Diffraction Study

The XRD patterns of NFPO nanoparticles were done using Cu-K_α radiation (1.5406 Å). XRD spectra confirmed (JCPDS file no. 86-2267) the cubic spinel phase formation of the NFPO nanoparticles, along with some extra peaks after $x = 0.025$. These extra peaks are of Pr_9O_{16} (praseodymium oxide) orthic phase (JCPDS file no. 83-1193), shows limitation for Pr^{3+} accommodation in spinel structure [21]. The increase in the intensity of these extra peaks with Pr ion doping shows that the amount of an orthic phase has been increased. The calculated crystallite size (D) was found to be in the range of 39–44 nm using Scherrer's formula as given below in equation (1)

$$D = \frac{0.9\lambda}{\beta \cos\theta} \tag{1}$$

And lattice parameter (a) was calculated using equation (2) given below.

$$a = \frac{\lambda}{2\sin\theta}\sqrt{h^2 + k^2 + l^2} \tag{2}$$

where λ is the wavelength of x-ray used, β is the full-width half maxima, and h, k and l are the Miller indices of the plane corresponding to the angle θ of highest intensity peak.

All Pr-doped samples have a larger crystallite size than pure nickel ferrite as rare earth ions are usually present at grain boundaries that cause hindrance to the grain growth, therefore, crystallite size increases [22]. Lattice parameter (a) and crystallite size (D) calculated from XRD data are shown in Table 1. All samples have nearly same lattice parameter except P1.

Table 1 Various parameters calculated from XRD and PPMS analysis

Sample name	Crystallite size (nm)	Lattice constant (Å)	$T = 300$ K		$T = 10$ K	
			M_S (emu/gm)	H_C (Oe)	M_S (emu/gm)	H_C (Oe)
P0	39.2	8.334	44	30	48	72
P1	44.3	8.353	41	44	44	67
P2	40.8	8.321	42	55	46	77
P3	41.2	8.311	50	57	56	129
P4	41.9	8.321	50	63	56	87

The lattice constant increases first from P0 to P1 which is similar to the results reported earlier [17]. This increase of lattice constant is due to the replacement of Fe^{3+} ion of radius (0.645 Å) by Pr^{3+} of radius (1.013 Å) at B-site. This replacing of a Fe^{3+} ion by Pr^{3+} large ion leads to an expansion of the unit cell and hence lattice parameter increases. After P1, it starts decreasing, and P2–P4 have comparable lattice parameter which is slightly lesser than P0. This is due to an extra phase formation after P1. All Pr^{3+} ions do not replace Fe^{3+} ions, but starts to diffuse on the grain boundaries to form Pr_9O_{16} phase. A pressure is generated around the grain boundary by a thin layer of this foreign phase, which results in the decrease in the lattice parameter [23] (Fig. 1).

3.2 EDX Analysis

The elemental and chemical composition has been analysed by EDX. The EDX spectrum confirmed that the Pr/Ni atomic ratio increases with increment in the doping of Pr. In addition, the atomic ratio of Ni/(Fe + Pr) was found close to the normal estimated values. No impurity peaks have been found (Fig. 2).

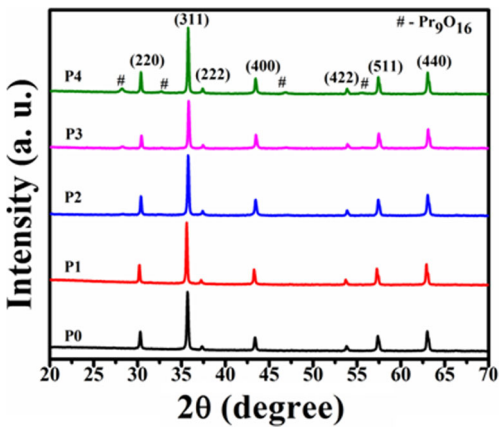

Fig. 1 X-ray diffraction pattern of the samples P0–P4

3.3 FTIR Study

Four main peaks are observed here in our sample in the range of 400–4000 cm^{-1}. As in ferrite's spinel structure, tetrahedral and octahedral sites are occupied by metal ions due to these two main bands are observed below 600 cm^{-1}. These bands are related to the vibration of ions in the different sites, A and B of the spinel structure. The stretching vibration of a unit cell of spinel in tetrahedral A site creates a band at higher (1) frequency while metal-oxygen vibration in octahedral sites creates a band at lower (2) frequency [24]. The low frequency band is not appearing in our samples, due to frequency limit 400 cm^{-1}. As we know, Pr^{3+} ions replace Fe^{3+} at the octahedral site, it will change the Fe–O stretching vibration. There is a difference between Fe–O and Pr–O bond length due to which peaks at the tetrahedral site around (530 cm^{-1}) shift towards higher wavenumber side [13], as listed in Fig. 3b.

The broad peak between 3200 and 3600 cm^{-1} and a small peak at around 1620 cm^{-1} may be attributed to the O–H vibration of water [25]. The bands are related to metal carbonate structures are observed at 1485 and 1361 cm^{-1} [26]. The intensity of these two absorptions is high in the case of RE doped ferrites (1485 in P2, P3 and P4 in our samples) is related to their ability to form surface carbonate structure [27].

3.4 TEM Analysis

TEM images of as-prepared samples corresponding to $X = 0$, 0.025, 0.05, 0.075 and 0.1 are shown in Fig. 4. Interesting shape change was observed for samples P0 to P4. Nano-octahedrons shape was observed in the case of P0 and P1 samples. Growth of nanorods of high aspect ratio are observed in P2, P3 and P4 along with nano-octahedrons as shown in TEM images. The change in morphology may be due to the foreign phase formation or change in nucleation rate by adding rare earth ions in ferrite structure [28]. Addition of Pr3+ ions first accelerates the nucleation and particle growth (as confirmed by XRD data crystallite size

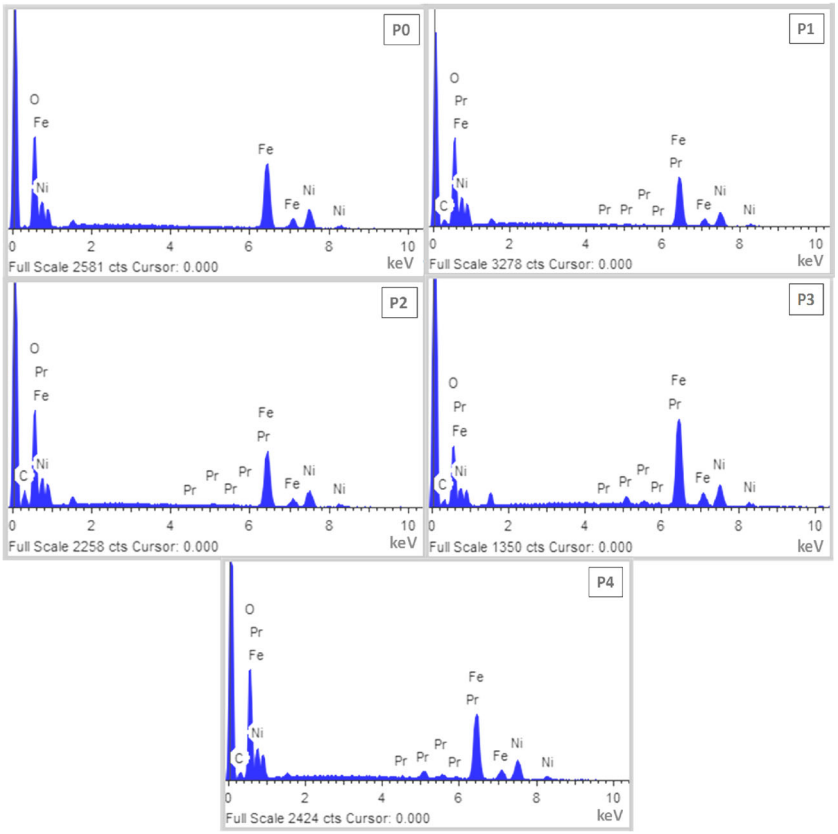

Fig. 2 EDX spectra of the samples

increases) from P0 to P1 result also. So, the morphology of the samples is changed by addition of Pr ions in spinel structure (Fig. 4).

3.5 Physical Properties Measurement System Analysis

Magnetic-hysteresis curves of all the samples (P0–P4) measured at 10 K and room temperature (300 K) using PPMS are shown in Fig. 5. The values of magnetic properties like, saturation magnetization (M_S) and coercivity (H_C) are listed in Table 1. At room temperature, the value of saturation magnetization first decrease P0 to P1 and then starts increases up to P4; same trend is observed at 10 K. Generally, magnetic properties are very sensitive to particle size, morphology and cation distribution [11, 29]. So, this can be explained by assuming that Pr^{3+} ions are occupying B site by replacing Fe^{3+} ions. As total magnetization is given by

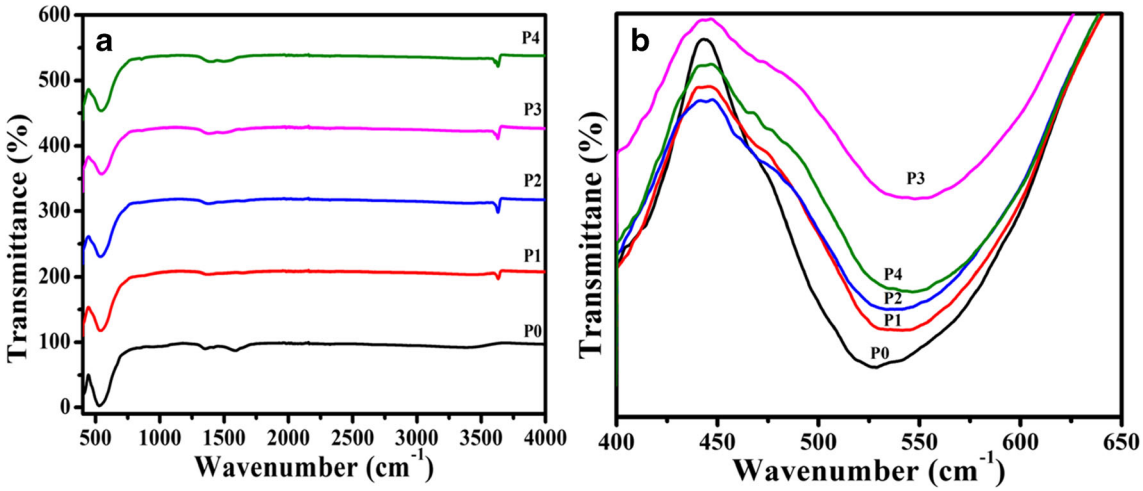

Fig. 3 FTIR spectra for samples P0–P4 in range **a** 400 to 4000 cm^{-1} and **b** 400 to 650 cm^{-1}

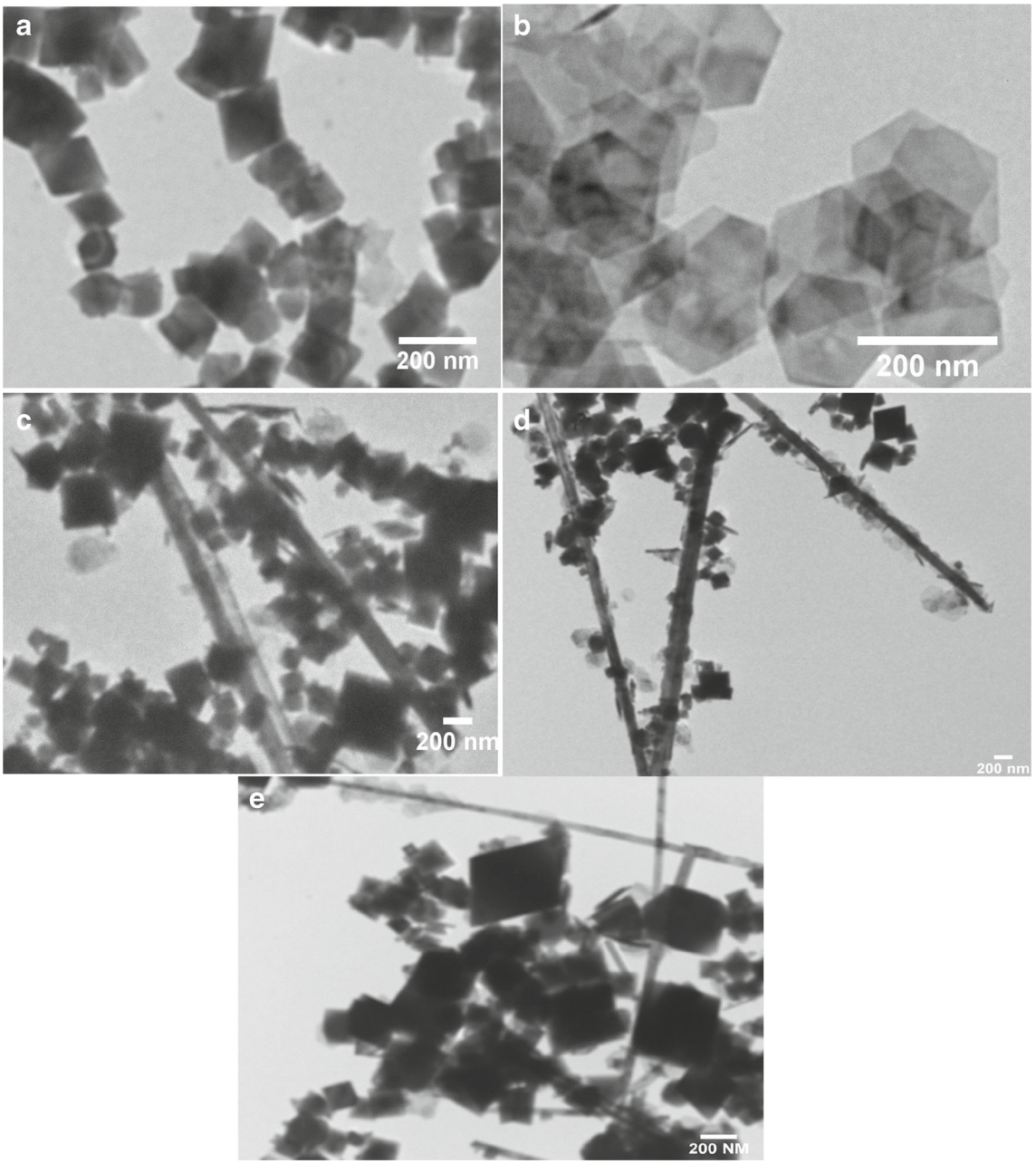

Fig. 4 TEM images of the samples **a** P0, **b** P1, **c** P2, **d** P3 and **e** P4

$M = |M_B - M_A|$and Pr^{3+} having a low magnetic moment (3.5 μB) are replacing high magnetic moment ions Fe^{3+} (5 μB), so M_B decreases and hence total magnetization decreases. After P1, M_S again starts to increase. As after P1, Pr^{3+} ions are no more replacing Fe^{3+} ions, but started to form an extra phase, so M_S again starts to increase after P1. This formation of extra phase leads the vacancy of Fe^{3+} ions in the spinel phase due to decreases in the molar ratio of Fe ions with respect to Ni ions in the samples P2–P4. This vacancy is created at the tetrahedral site as lattice parameter is decreased after P1; in this way, magnetic moment at A site decreases, which leads to increase in M_S value.

Coercivity at room temperature is found to be increasing from P0 to P4. Impurities distributed in the grain boundary area break and go against the displacement of domain walls. Due to the existence of the foreign phase Pr_9O_{16} and the like, the samples after doping with more Pr^{3+} ions were expected to have larger coercivity as shown in Table 1. Similar behaviour was observed earlier [13]. At 10 K, the value of the coercivity is increased from P0 to P4 but does

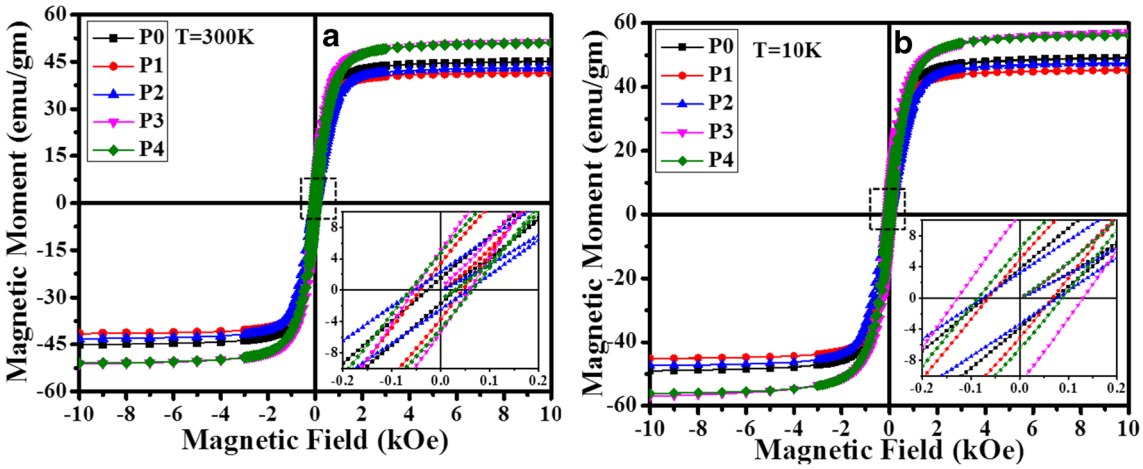

Fig. 5 Hysteresis loops measured at **a** room temperatures and **b** hysteresis loops measured at K; for all the samples

not follow the same trend as in room temperature shown in Table 1. It is found that P_3 has the highest coercivity (129 Oe).

A comparative study of magnetic behaviour of the present work with literature has been shown in Table 2. We found that our samples have low coercivity with high-saturation magnetization value and can be used as soft magnetic materials. The observed values of these magnetic parameters makes them very useful for biomedical applications like magnetic resonance imagining (MRI), magneto-resistive sensors, antibacterial and catalyst.

4 Conclusions

The nickel ferrite nanoparticles with different doping amounts of Pr^{3+} ions were successfully synthesized by hydrothermal method. From the XRD data, we concluded that main phase of spinel ferrite was formed along with small amount of an orthic phase (Pr_9O_{16}) after $X = 0.025$ which was due to solubility limit for Pr^{3+} ions substitution in spinel ferrite. The crystallite size and lattice parameter were first increases from P0 to P1 due to the expansion of unit cell by replacement of small Fe^{3+} ions by larger Pr^{3+} ions. After P1, it again started to decrease; P2, P3, and P4 have nearly same (comparable to P0) crystallite size and lattice parameter due to pressure generated around the grain boundary by a thin layer of Pr_9O_{16} foreign phase. The nanoparticles of P0 and P1 samples have nano-octahedron morphology, but P3–P5 samples were a mixture of nanorods of high aspect ratio along with nano-octahedrons which may be due enhanced in nucleation rate or due to extra phase formation by increasing doping amount. The saturation magnetization of the samples was first decreased from P0 to P1 replacement of Fe^{3+} ions of the high magnetic moment by Pr^{3+} ions of a low moment. Then, it again starts increasing up to P4 at room temperature and 10 K. This may be due to Pr^{3+} ions no longer replacing the Fe^{3+} ions as may be due to the extra phase formation and a vacancy is created at A site due to smaller molar ratio of Fe ions with respect to Ni^{2+}. The coercivity was increased from P0 to P4 at room temperature and 10 K impurities distributed in the grain boundary area break and go against the displacement of domain walls, but P3 was the exemption at 10 K.

Table 2 Comparison of change in magnetic properties of NFO by adding different rare earth ions

Rare earth ion (Re) present in $NiFe_{2-X}Re_XO_4$	Range of doping amount (x)	Range of M_S (emu/gm)	Range of H_C (Oe)	Reference number
Sm	0–0.15	33–52	46–81	[30]
Nd	0–0.03	50.9–59.8	151–99	[31]
Ce	0–0.1	31.64–42.9	67.7–5.9	[32]
Pr	0–0.1	41–50	30–63	Present work

Acknowledgements The authors would like to thank IIT Delhi for characterization facilities.

Funding Information The authors would like to thank the Univ. Grant Commission (UGC), Govt. of India, for financial support.

References

1. Darshane, S.L., Suryavanshi, S.S., Mulla, I.S.: Nanostructured nickel ferrite: a liquid petroleum gas sensor. Ceram. Int. **35**, 1793–1797 (2009)
2. Chunga, Y.S., Park, S.B., Kang, D.W.: Magnetically separable titania-coated nickel ferrite photocatalyst. Mater. Chem. Phys. **86**, 375–381 (2004)
3. Zhu, W., Wang, L., Zhao, R., Ren, J., Lua, G., Wang, Y.: Electromagnetic and microwave-absorbing properties of magnetic nickel ferrite nanocrystals. Nanoscale **3**, 2862–2864 (2011)
4. Singh, A.K., Srivastava, O.N., Singh, K.: Shape and size-dependent magnetic properties of Fe_3O_4 nanoparticles synthesized using piperidine. Nanoscale Res. Lett. **12**, 298 (2017)
5. Gyergyek, S., Makovec, D., Iztok Arcon, A.K., Jagodic, M., Drofenik, M.: Influence of synthesis method on structural and magnetic properties of cobalt ferrite nanoparticles. J. Nanopart. Res. **12**(4), 1263–1273 (2010)
6. Aakash, R.C., Das, D., Mukherjee, S.: Effect of doping of manganese ions on the structural and magnetic properties of nickel ferrite. J. Alloys Compd. **668**, 33–39 (2016)
7. Chakrabarty, S., Dutta, A., Pal, M.: Enhanced magnetic properties of doped cobalt ferrite nanoparticles by virtue of cation distribution. J. Alloys Compd. **625**, 216–223 (2015)
8. Rezlescu, N., Rezlescu, L., Popa, P.D., Rezlescu, E.: Influence of additives on the properties of a Ni–Zn ferrite with low Curie point. J. Magn. Magn. Mater. **215–216**, 194–196 (2000)
9. Mahalakshmi, S., Srinivasa, M.K., Nithiyanantham, S.: Electrical properties of nanophase ferrites doped with rare earth ions. J. Supercond. Novel Magn. **27**, 2083–2088 (2014)
10. Bharathi, K.K., Ramana, C.V.: Improved electrical and dielectric properties of La-doped Co ferrite. J. Mater. Res. **26**, 584–591 (2011)
11. Heiba, Z.K., Mohamed, M.B., Arda, L., Dogan, N.: Cation distribution correlated with magnetic properties of nanocrystalline gadolinium substituted nickel ferrite. J. Magn. Magn. Mater. **391**, 195–202 (2015)
12. Bharathi, K.K., Chelvane, J.A., Markandeyulu, G.: Magnetoelectric properties of Gd and Nd-doped nickel ferrite. J. Magn. Magn. Mater. **321**, 3677–3680 (2009)
13. Wua, X., Wang, W., Song, N., Yang, X., Khaimanov, S., Tsidaeva, N.: From nanosphere to nanorod: tuning morphology, structure and performance of cobalt ferrites via pr^{3+} doping. J. Chem. Eng. **306**, 382–392 (2016)
14. Liua, Z., Penga, Z., Lv, C., Fu, X.: Doping effect of sm^{3+} on magnetic and dielectric properties of Ni-Zn ferrites. Ceram. Int. **43**, 1449–1454 (2017)
15. Rao, P., Godbole, R.V., Bhagwat, S.: Chlorine gas sensing performance of palladium doped nickel ferrite thin films. J. Magn. Magn. Mater. **405**, 219–224 (2016)
16. Rezlescu, N., Rezlescu, E., Pasnicu, C., Craus, M.L.: Effects of the rare-earth ions on some properties of a nickel-zinc ferrite. J. Phys.: Condens. Matter. **6**, 5707–5716 (1994)
17. Raju, P., Murthy, S.R.: Preparation and characterization of Ni–Zn ferrite + polymer nanocomposites using mechanical milling method. Appl. Nanosci. **3**, 469–475 (2013)
18. Huang, X., Zhang, J., Lai, M., Sang, T.: Preparation and microwave absorption mechanisms of the NiZn ferrite nanofibers. J. Alloys Compd. **627**, 367–373 (2015)
19. Haque, S.U., Saikia, K.K., Murugesan, G., Kalainathan, S.: A study on dielectric and magnetic properties of lanthanum substituted cobalt ferrite. J. Alloys Compd. **701**, 612–618 (2017)
20. Byrappa, K., Adschiri, T.: Hydrothermal technology for nanotechnology. Prog. Cryst. Growth Charact. Mater. **53**, 117–166 (2007)
21. Şabikoğlua, İ., Paralb, L., Malinac, O., Novakc, P., Kaslikc, J., Tucekc, J., Pechousekc, J., Navarikc, J., Schneeweissd, O.: The effect of neodymium substitution on the structural and magnetic properties of nickel ferrite. Mater. Int. **25**, 215–221 (2015)
22. Pervaiza, E., Gula, I.H.: Structural, electrical and magnetic studies of gd^{3+} doped cobalt ferrite nanoparticles. Int. J. Curr. Eng. Technol. **2**(4), 377–387 (2012)
23. Rady, K.E., Shamsb, M.S.: Study the effect of gd^{3+} incorporation into nanocrystalline (Ni–Ti) substituted Mn–Zn ferrites on its structure and functional properties. J. Magn. Magn. Mater. **426**, 615–620 (2017)
24. Waldron, R.D.: Infrared spectroscopy of ferrites. Phys. Rev. **99**, 1727 (1955)
25. Zhao, L., Yang, H., Zhao, X., Yu, L., Cui, Y., Feng, S.: Magnetic properties of $CoFe_2O_4$ ferrite doped with rare earth ion. Math. Lett. **60**, 1–6 (2006)
26. Abu-Zied, B.M., Soliman, S.A., Abdellah, S.E.: Enhanced direct N_2O decomposition over $Cu_xCo_{1-x}Co_2O_4$ ($0.0 < x < 1.0$) spinel-oxide catalysts. J. Ind. Eng. Chem. **21**, 814–821 (2015)
27. Abu-Zied, B.M., Bawaked, S.M., Kosa, S.A., Schwieger, W.: Impact of Gd-, La-, Nd- and Y-doping on the textural, electrical conductivity and N_2O decomposition activity of CuO catalyst. Int. J. Electrochem. Sci. **11**, 2230–2246 (2016)
28. Xiang, J., Shen, X., Song, F., Liu, M.: One-dimensional NiCuZn ferrite nanostructures: fabrication, structure, and magnetic properties. J. S. Stat. Chem. **183**, 1239–1244 (2010)
29. Jankovský, O., Rach, V., Sedmidubský, D., Huber, S., Ulbrich, P., Svecov, M., Bartunek, V.: Simple synthesis of free surface nanostructured spinel $NiFe_2O_4$ with a tunable particle size. J. Alloys Compd. **723**, 58–63 (2017)
30. Hassanzadeh-Tabrizi, S.A., Behbahanian, S., Amighian, J.: Synthesis and magnetic properties of $NiFe_{2-x}Sm_xO_4$ nanopowder. J. Magn. Magn. Mater. **410**, 242–247 (2016)
31. Shinde, T.J., Gadkari, A.B., Vasambekar, P.N.: Influence of Nd3+ substitution on structural, electrical and magnetic properties of nanocrystalline nickel ferrites. J. Alloys Compd. **513**, 80–85 (2012)
32. Dixit, G., Singh, J.P., Srivastava, R.C., Agrawal, H.M.: Structural, optical and magnetic studies of Ce doped $NiFe_2O_4$ nanoparticles. J. Magn. Magn. Mater. **345**, 65–71 (2013)